

**Intrinsic Absorption Lines in the Seyfert 1 Galaxy NGC 5548:
UV Echelle Spectra from the Space Telescope Imaging
Spectrograph¹**

D. Michael Crenshaw^{2,3} and Steven B. Kraemer^{2,4,5}

Received 1998 December 23; accepted 1999 March 29

¹Based on observations with the NASA/ESA *Hubble Space Telescope*, which is operated by the Association of Universities for Research in Astronomy, Inc., under NASA contract NAS5-26555.

²Catholic University of America and Laboratory for Astronomy and Solar Physics, NASA's Goddard Space Flight Center, Code 681 Greenbelt, MD 20771.

³Email: crenshaw@buckeye.gsfc.nasa.gov.

⁴Email: stiskraemer@yancey.gsfc.nasa.gov.

⁵Space Telescope Imaging Spectrograph (STIS) Instrument Definition Team

ABSTRACT

We present the first observations of a Seyfert galaxy with the echelle gratings on the Space Telescope Imaging Spectrograph (STIS), which provide high-resolution ($\lambda/\Delta\lambda \approx 40,000$) coverage of the intrinsic UV absorption lines in NGC 5548. We confirm the presence of five kinematic components of absorption in $\text{L}\alpha$, C IV, and N V at radial velocities of -160 to -1060 km s^{-1} with respect to the emission lines, and find an additional $\text{L}\alpha$ component near the systemic velocity, which probably arises in the interstellar medium of the host galaxy. Compared to GHRS spectra of the N V and C IV absorption obtained ~ 2 years earlier, the kinematic components have not changed in radial velocity, but the ionic column densities for two components have decreased. We attribute these variations to changes in the total column of gas, but for one component, we cannot rule out changes in the ionization of the gas.

We have calculated photoionization models to match the UV column densities from each of the five components associated with the nucleus. In four of the components, the ionization parameters ($U = 0.15 - 0.80$) and effective hydrogen column densities ($N_{\text{eff}} = 6.0 \times 10^{18} \text{ cm}^{-2} - 2.8 \times 10^{20} \text{ cm}^{-2}$) cannot produce the O VII and O VIII absorption edges seen in the X-ray warm absorber. The remaining component is more highly ionized ($U = 2.4$, $N_{\text{eff}} = 6.5 \times 10^{21} \text{ cm}^{-2}$) and our model matches the previously observed X-ray absorption columns. This component is therefore likely to be responsible for the X-ray warm absorber. It also has the highest outflow velocity and showed the largest variations in column density.

Subject headings: galaxies: individual (NGC 5548) – galaxies: Seyfert

1. Introduction

With the advent of the *Hubble Space Telescope* (HST), it has become clear that intrinsic absorption is a common phenomenon in the UV spectra of Seyfert 1 galaxies. From a study of HST archive spectra, we determined that $\sim 60\%$ (10/17) of the Seyfert 1 galaxies in our sample have intrinsic absorption lines (Crenshaw et al. 1999). All ten of the Seyferts with absorption showed high ionization lines (N V $\lambda\lambda 1238.8, 1242.8$; C IV $\lambda\lambda 1548.2, 1550.8$), in addition to $\text{Ly}\alpha$. Low ionization lines were less common: four Seyferts showed detectable Si IV $\lambda\lambda 1393.8, 1402.8$ absorption, and only one showed Mg II absorption $\lambda\lambda 2796.3, 2803.5$ absorption (NGC 4151). The intrinsic absorption lines are blueshifted by up to 2100 km s^{-1} with respect to the narrow emission lines, which indicates net radial outflow of the absorbing gas. At high spectral resolution, the lines often split into distinct narrow components, with widths in the range $20 - 400 \text{ km s}^{-1}$ (FWHM).

Intrinsic absorption is also common in the X-ray spectra of Seyfert galaxies; about half of these objects show “warm absorbers”, characterized by O VII and O VIII absorption edges (Reynolds 1997; George et al. 1998). We found a clear correspondence between the UV and X-ray absorption in our survey; of the eight Seyferts that were observed by both *HST* and *ASCA*, six showed both UV and X-ray absorption and two showed neither (Crenshaw et al. 1999). Mathur and collaborators first established a connection between the UV and X-ray absorbers, and claimed that a single zone of photoionized gas can explain both the observed strengths of O VII and O VIII absorption edges and the UV absorption lines in quasars (Mathur 1994) and the Seyfert galaxy NGC 5548 (Mathur et al. 1995). However, in NGC 4151 (Kriss et al. 1998) and NGC 3516 (Kriss et al. 1996; Crenshaw et al. 1998), multiple zones spanning a wide range in ionization parameter and effective hydrogen column density are needed to explain the wide range in ionization species and large column densities of the UV absorption lines.

Since the intrinsic UV absorption in a Seyfert 1 galaxy is typically comprised of multiple kinematic components, an obvious question arises: are these components characterized by different physical conditions? An important related question is: to what extent do the UV and X-ray absorbers arise in the same regions? In order to address these issues, near-simultaneous high-resolution spectra of multiple lines are needed, to determine the column densities of different ions for each component. The only data that have met these requirements are the Goddard High Resolution Spectrograph (GHRS) observations of the C IV and Mg II absorption in NGC 4151 (Weymann et al. 1997; Kriss 1998). The C IV/Mg II column density ratio varies widely in this object, indicating a broad range in ionization parameter among the different kinematic components.

The Space Telescope Imaging Spectrograph (STIS) on *HST* offers an important means for investigating the differences in physical conditions among different kinematic components, by providing echelle gratings that cover broad bandpasses in the UV at a resolution of $\lambda/\Delta\lambda \approx 40,000$. To take advantage of this capability, we initiated a STIS Guaranteed Time Observations (GTO) program to obtain echelle spectra of several Seyfert 1 galaxies. Our first target is NGC 5548.

2. Observations and Analysis

We obtained STIS echelle spectra of the nucleus of NGC 5548 on 1998 March 11 through the $0''.2 \times 0''.2$ aperture. The observations are described in Table 1, along with previous GHRS observations of the N V and C IV regions obtained ~ 2 years earlier (the N V region contains a portion of the $L\alpha$ profile). We reduced the STIS echelle spectra using the IDL software developed at NASA's Goddard Space Flight Center for the STIS Instrument Definition Team (Lindler et al. 1998). The procedures that we followed to identify the Galactic and intrinsic absorption lines and measure the intrinsic lines are given

in Crenshaw et al. (1999).

Figure 1 shows the regions in the echelle spectra where the intrinsic absorption lines were detected ($\text{L}\alpha$, N V , and C IV), and the regions where the strongest low-ionization lines might be expected (Si IV , Mg II). The fluxes are plotted as a function of the radial velocity (of the strongest member for the doublets) relative to the emission-line redshift, $z = 0.01676$, obtained from the NASA/IPAC Extragalactic Database (NED). To obtain velocities relative to the redshift from H I observations ($z = 0.01717$), the velocity scale should be offset by an additional -123 km s^{-1} . $\text{L}\alpha$ shows six distinct kinematic components, and the first five components are also seen in the absorption doublets of N V and C IV at essentially the same radial velocities. The Si IV and Mg II regions show no obvious counterparts, but the spectra are important for putting upper limits on the column densities of these ions.

Components 1 – 5 are the same as those identified by Crenshaw et al. (1999) in the GHRs spectra. Component 6 can also be seen in the GHRs spectra of $\text{L}\alpha$, but was not identified in that paper. Mathur, Elvis, and Wilkes (1999) have also identified the velocity components in the GHRs spectra of C IV . Their identifications are the same as ours, except that they identify the dip in the red wing of component 4 as a separate component, and they identify the feature that we claim to be the $\text{C IV } \lambda 1550.8$ line of component 5 with the $\text{C IV } \lambda 1548.2$ line of a component that is slightly redshifted with respect to the systemic redshift. The feature that corresponds to the $\lambda 1550.8$ line of the redshifted component can be seen in the GHRs spectra (Crenshaw et al. 1999), but was too weak to satisfy our criteria for detection. We cannot identify this component in the STIS N V and C IV regions, but there is a weak feature at $+300 \text{ km s}^{-1}$ in the STIS $\text{L}\alpha$ region (Figure 1) that may correspond to Mathur et al.’s redshifted component. Due to the uncertainty about the existence of this component, we will not consider it further in this paper.

Comparing the STIS spectra with the GHRS spectra, we find that the absorption components are resolved in both. The higher resolution of the STIS spectra makes the velocity structure in some of the components, such as the dip in the red wing of component 4, more distinguishable. We note that the short-wavelength GHRS spectrum does not include the blue wing of the $\text{L}\alpha$ and the absorption from component 1. The GHRS spectrum of C IV has a substantially higher SNR, since the exposure time was ~ 3 times that of the STIS spectrum. Thus, the C IV absorption for component 1 is not apparent in the STIS spectrum, and we can only give an upper limit on its column density (see below).

Table 2 gives the radial velocity centroids, widths (FWHM), and covering factors in the line of sight for each component. The values and uncertainties that we present are averages and standard deviations from individual lines; measurements of the individual lines and the Galactic lines will be given in another paper (Sahu et al. 1999). The methods for determining the measurement errors are described in Crenshaw et al. (1999), and include uncertainties due to different reasonable placements of the underlying emission. For each component, two lower limits are given for the covering factor in the line of sight: C_{los} , which is the fraction of total emission (continuum plus broad-line emission) that is occulted, and C_{los}^{BLR} , which is the fraction of broad-line emission that is occulted (assuming the entire continuum source is occulted). These lower limits have been determined from the residual intensities in the $\text{L}\alpha$ cores (see Crenshaw et al. 1999).

A comparison of the measurements in Table 2 with those from the GHRS spectra (Crenshaw et al. 1999) shows that, to within the errors, there have been no changes in the velocity centroids or widths of the components over ~ 2 years. The lower limits to the covering factors are essentially the same as those obtained from the GHRS spectra. For components 1–5, both the total covering factor, C_{los} , and the BLR covering factor, C_{los}^{BLR} , are greater than one-half and in some cases, close to one. We can conclude that each of

the components is likely to be outside of the BLR and comparable in size to or larger than the BLR in the plane of the sky. Component 6 shows weak $\text{L}\alpha$ absorption, is not detected in the other lines, and is located close to the systemic velocity of the host galaxy, which suggests that the gas responsible for this component is associated with the interstellar medium of the host galaxy. We will not discuss this component further.

In Table 3, we give the column densities of $\text{L}\alpha$, N V , and C IV for each component. Since we only have lower limits to the covering factors, these values were determined by assuming that $C_{\text{los}} = 1$, and integrating the optical depths as a function of radial velocity across each component (see Crenshaw et al. 1999 for a discussion of the effects of $C_{\text{los}} \neq 1$ on the measured column densities). The blending of the $\text{L}\alpha$ components in Figure 1 indicates that they are more saturated than the other lines, and therefore the column densities are affected by the deblending of the components and by errors in the removal of scattered light. The uncertainties in the $\text{L}\alpha$ columns in Table 3 are due to measurement errors, and do not include these effects.

Table 3 shows that there have been significant decreases in the N V column densities for components 1 and 3, and a possible decrease in the C IV column density for component 3, since the GHRS observations from ~ 2 years earlier. These changes are also apparent in a comparison of Figure 1 with the GHRS spectra in Crenshaw et al. (1999). Since we only have an upper limit for the C IV column density of component 1, we have no information on its variability. The other components have not changed, given the uncertainties.

To compare our results with those obtained for the X-ray warm absorber in NGC 5548, we use the *ASCA* observations of this Seyfert on 1993 July 27 (Reynolds 1997; George et al. 1998). From the optical depths of the O VII and O VIII absorption edges in Reynolds and the ionization cross sections, we calculate column densities of 1.0×10^{18} and $1.6 \times 10^{18} \text{ cm}^{-2}$ for O VII and O VIII , respectively.

3. Photoionization Models

We have generated photoionization models to investigate the physical conditions in the absorption components. The details of the photoionization code are described in Kraemer et al. (1994, and references therein). Most of the input parameters for these models (e.g., solar abundances) are identical to those used in our previous study of the narrow emission line region (NLR) in NGC 5548 (Kraemer et al. 1998). We have modeled the ionizing continuum as a broken power-law, $L_\nu = K\nu^\alpha$, with the following spectral indices: $\alpha = -1.0$ ($h\nu < 13.6$ eV), $\alpha = -1.4$ (13.6 eV $\leq h\nu < 1300$ eV), and $\alpha = -0.9$ ($h\nu \geq 1300$ eV). Note that we have modified the value of α above 1.3 keV from that used in Kraemer et al. (1998), based on Reynolds’s (1997) fit to the 2 – 10 keV continuum.

The parameters that we varied in generating our photoionization models were the ionization parameter U (the number of ionizing photons per hydrogen atom at the illuminated face of the cloud), and the effective hydrogen column density N_{eff} (i.e., the neutral plus ionized hydrogen column). The ionic column densities predicted by the models do not depend on the atomic density, n_H . For simplicity we chose a fixed value of $n_H = 5 \times 10^5$ cm $^{-3}$; at the distance of our innermost component in the NLR models (~ 1 pc, see Kraemer et al. 1998), this yields a value of $U = 0.60$, which is approximately correct for producing the observed ratios of N V to C IV. We generated a single model for each kinematic component, by varying U until the N V/C IV column ratio was matched. We then adjusted N_{eff} to fit the ionic column densities. We varied these parameters until the predicted columns matched the observed values to within the errors. Due to our concerns about the $L\alpha$ column densities (see the previous section), we did not use these columns to constrain the models.

The model values for components 2 – 5 are listed in Table 4. Since we only have an upper limit to the C IV column density for component 1 in the STIS data, we will

treat that case separately. The predicted column densities for Si IV and Mg II are well below detectability in all cases; the largest value computed for Si IV was $\sim 4 \times 10^9 \text{cm}^{-2}$ (component 4), and the Mg II column was effectively zero for all components. Despite our concerns about the observed H I columns, the observed and predicted values are reasonably close; the predicted values tend to be higher (by up to a factor of ~ 2.4 for component 4). One possible explanation is that our $\text{Ly}\alpha$ measurements are indeed affected by saturation effects; another is that the abundances are greater than solar by a factor of two⁶. The values of U and N_{eff} that we obtain for these components are well below those associated with typical X-ray warm absorbers ($U = 1 - 10$, $N_{\text{eff}} = 10^{21} - 10^{23} \text{cm}^{-2}$; Reynolds 1997; George et al. 1998). To investigate this issue further, we computed column densities for O VII and O VIII, which are also listed in Table 4. The total predicted columns for these ions are $1.6 \times 10^{17} \text{cm}^{-2}$ and 9.9×10^{15} , whereas the observed values are ~ 6 and ~ 160 times higher for O VII and O VIII, respectively, which shows that components 2 – 5 do not contribute significantly to the X-ray warm absorber.

For component 3, the N V and C IV column densities have decreased by about the same amount in the STIS data (factor of ~ 1.6) compared to the GHRS observations (Table 2). This would indicate that the ionization parameter was essentially the same on these two occasions. Thus, the most likely explanation for the absorption changes is that the effective column density changed, due to bulk motion of some of the absorbing gas out of the line of sight. A possible discrepancy with this interpretation is that the H I column density did

⁶Since this is the first time that we have run models in this high-ionization regime, we compared our calculations with those from CLOUDY90 (Ferland et al. 1998). The ionic column densities for the high ionization lines were quite similar, and the H I columns from CLOUDY were a factor of ≤ 2 higher than ours (due to a different treatment of the cooling), which indicates that our overprediction of the H I columns is not a model artifact.

not change appreciably, but we have already noted the difficulties involved in determining the H I columns from $L\alpha$.

For component 1, we generated a model based on the GHRS column densities. Table 5 shows these values. Due to the large N V/C IV ratio, the ionization parameter and effective column density for this component are much higher than those for the other components. The predicted O VII and O VIII column densities are very close to the observed values, suggesting that this component is likely to be responsible for the X-ray warm absorber. Our values of U and N_{eff} for this component are similar to those determined for the warm absorber in NGC 5548 by Reynolds (1997) and George et al. (1998). With the caveat that none of the UV or X-ray observations are simultaneous, we conclude that component 1 is likely to be the X-ray warm absorber.

To investigate the column density variations in component 1, we generated two additional models for the STIS data, as shown in Table 5. For the first model, we assumed that U did not change between the two observations, and for the second model, we assumed that N_{eff} remained constant. Both models match the observed N V column density, predict a low C IV column, and overpredict the neutral hydrogen column. Thus, the difference in ionic column densities between the GHRS and STIS data for Component 1 could be simply explained by: 1) an increase of U by a factor of ~ 1.4 , or 2) a decrease of N_{eff} by a factor of ~ 4 along the line of sight. We prefer the latter explanation, since the discrepancy between the observed and predicted neutral hydrogen columns is similar to that for the other components, but cannot rule out the former.

4. Conclusions

We have obtained UV echelle spectra of NGC 5548 with STIS, and have confirmed the presence of five kinematic components of intrinsic absorption in the lines of $\text{L}\alpha$, C IV, and N V. An additional $\text{L}\alpha$ component is present near the systemic redshift, and is likely to be associated with the interstellar medium in the host galaxy. These components have not changed in their radial velocity coverage since the GHRS observations ~ 2 years earlier. The column densities of N V and C IV in component 3 have decreased, and the column density of N V in component 1 has decreased over the two year interval (only an upper limit is available for component 1's C IV column in the STIS data).

We have used photoionization models to examine the physical conditions in the gas responsible for the intrinsic absorption. The ionization parameters and effective column densities for components 2 – 5 are lower than those associated with X-ray warm absorbers, and the predicted O VII and O VIII column densities for these components are too small to make a significant contribution to the X-ray absorption. From the GHRS observations of N V and C IV, we obtain much higher values of U (2.4) and N_{eff} ($6.5 \times 10^{21} \text{ cm}^{-2}$) for component 1. Our predicted O VII and O VIII columns for component 1 match the previous observed values. We conclude that this component is likely to be responsible for the X-ray warm absorber. This component also has the highest outflow velocity and exhibits the strongest variability. Since the GHRS C IV and N V spectra were obtained ~ 6 months apart, and the *ASCA* observations were obtained ~ 3 years earlier, these conclusions need to be checked with simultaneous UV and X-ray observations.

We find that the decrease in the N V and C IV column densities in component 3 is due to a change in the total column density of the absorption, rather than a change in ionization, since the N V/C IV ratio did not change significantly. This is the most likely explanation for the decrease in N V column in component 1 as well, although we cannot

rule out a change in ionization. Assuming that bulk motion of the gas across the line of sight is responsible for the variations, complete coverage of the BLR, and a diameter of the N V emitting region of ~ 4 light days (Korista et al.), we find a transverse velocity of $v_T \geq 1650 \text{ km s}^{-1}$. If the variations are due to bulk motion, these two components have transverse velocities which are comparable to their outflow velocities.

We thank Ian George for helpful discussions on the X-ray absorption. D.M.C. and S.B.K. acknowledge support from NASA grant NAG 5-4103. Support for this work was provided by NASA through grant number NAG5-4103 and grant number AR-08011.01-96A from the Space Telescope Science Institute, which is operated by the Association of Universities for Research in Astronomy, Inc., under NASA contract NAS5-26555.

REFERENCES

- Crenshaw, D.M., Maran, S.P., & Mushotzky, R.F. 1998, *ApJ*, 496, 797
- Crenshaw, D.M., et al. 1999, *ApJ*, in press.
- George, I.M., 1998, *ApJS*, 114, 73
- Ferland, G.F., et al. 1998, *PASP*, 110, 761
- Korista, K.T., et al. 1995, *ApJS*, 97, 285
- Kraemer, S.B., Crenshaw, D.M., Peterson, B.M., and Filippenko, A.V. 1998, *ApJ*, 499, 719
- Kraemer, S.B., Wu, C.-C., Crenshaw, D.M., & Harrington, J.P. 1994, *ApJ*, 435, 171
- Kriss, G.A. 1998, in *The Scientific Impact of the Goddard High Resolution Spectrograph*, ed. J.C. Brandt, T.B. Ake III, and C.C. Peterson, (San Francisco: Astronomical Society of the Pacific) ASP Conference Series, 143, 271
- Kriss, G.A., et al. 1996, *ApJ*, 467, 622
- Lindler, D. 1998, *CALSTIS Reference Guide* (CALSTIS Version 5.1)
- Mathur, S. 1994, *ApJ*, 431, L75
- Mathur, S., Elvis, M., & Wilkes, B. 1999, *ApJ*, in press
- Mathur, S., Elvis, M., & Wilkes, B. 1995, *ApJ*, 452, 230
- Reynolds, C.S. 1997, *MNRAS*, 286, 513
- Sahu, M.S., Bruhweiler, F.C., Kraemer, S.B., & Crenshaw D.M. 1999, in preparation
- Savage, B.D., Sembach, K.R., & Lu, L. 1997, *AJ*, 113, 2158
- Weymann, R.J., Morris, S.L., Gray, M.E., & Hutchings, J.B. 1997, *ApJ*, 483, 717

Fig. 1.— Portions of the *STIS* UV echelle spectra of NGC 5548, showing the intrinsic absorption lines. Fluxes are plotted as a function of the radial velocity (of the strongest member, for the doublets), relative to an emission-line redshift of 0.01676. The kinematic components are identified with large numbers. Galactic lines are indicated with a “G”, and the small numbers identify the weak members of the doublets. Fits to the emission profile are given as dotted lines.

Table 1. High-Resolution UV Spectra of NGC 5548

Instrument	Grating	Coverage (Å)	Resolution ($\lambda/\Delta\lambda$)	Exposure (sec)	Date (UT)
STIS	E140M	1150 – 1730	46,000	4750	1998 March 11
STIS	E230M	1607 – 2366	30,000	2295	1998 March 11
STIS	E230M	2274 – 3119	30,000	1905	1998 March 11
GHRS	G160M	1232 – 1269 ^a	20,000	4607	1996 February 17
GHRS	G160M	1554 – 1590 ^b	20,000	13,600	1996 August 24

^aN V and a portion of $\text{Ly}\alpha$, Savage et al. 1997; Crenshaw et al. 1999

^bC IV, Crenshaw et al. 1999; Mathur et al. 1999

Table 2. Kinematic components and covering factors

Component	v_r ^a (km s ⁻¹)	FWHM (km s ⁻¹)	C_{los}	C_{los}^{BLR}
1	-1056 ± 27	85 ± 25	>0.62	>0.51
2	-669 ± 6	39 ± 9	>0.76	>0.71
3	-540 ± 16	78 ± 25	>0.90	>0.88
4	-340 ± 5	140 ± 5	>0.94	>0.93
5	-163 ± 25	75 ± 7	>0.63	>0.58
6 ^b	88 ± 5	63 ± 8	>0.23	>0.14

^aRelative to the emission-line redshift of 0.01676.

^bPresent only in $\text{Ly}\alpha$.

Table 3. Column densities in NGC 5548

Ion	Component	N (STIS) (10^{14} cm^{-2})	N (GHRS) (10^{14} cm^{-2})
L α	1	1.34 ± 0.16	——— ^a
L α	2	0.61 ± 0.12	0.76 ± 0.09
L α	3	2.01 ± 0.11	1.79 ± 0.21
L α	4	2.97 ± 0.12	3.30 ± 0.29
L α	5	0.66 ± 0.08	0.77 ± 0.11
L α	6	0.13 ± 0.04	0.13 ± 0.04
N V	1	0.44 ± 0.18	1.98 ± 0.29
N V	2	0.82 ± 0.16	0.57 ± 0.17
N V	3	2.33 ± 0.32	3.93 ± 0.27
N V	4	8.54 ± 0.65	6.47 ± 0.50
N V	5	1.18 ± 0.24	1.05 ± 0.23
C IV	1	<0.17	0.11 ± 0.04
C IV	2	0.34 ± 0.07	0.28 ± 0.04
C IV	3	0.30 ± 0.10	0.48 ± 0.15
C IV	4	2.95 ± 0.24	2.89 ± 0.22
C IV	5	0.31 ± 0.13	0.41 ± 0.18
Si IV		<0.10	
Mg II		<0.02	

^aNot included in wavelength coverage.

Table 4. Model Predictions for STIS Ionic Column Densities

Comp.	U	N_{eff} (cm^{-2})	H I	C IV	N V (10^{14} cm^{-2})	O VII	O VIII
2	0.15	6.0×10^{18}	0.72	0.35	0.85	20.10	1.26
3	0.80	2.8×10^{20}	3.77	0.32	2.53	1.16×10^3	56.20
4	0.20	8.3×10^{19}	7.05	2.97	8.46	3.28×10^2	28.23
5	0.30	2.2×10^{19}	1.11	0.33	1.25	1.15×10^2	13.70

Table 5. Model Predictions for Ionic Column Densities^a for Component 1

Source	U	N_{eff} (cm^{-2})	H I	C IV	N V (10^{14} cm^{-2})	O VII	O VIII
GHRS	2.42	6.5×10^{21}	14.60	0.11	2.02	1.05×10^4	2.29×10^4
STIS (U fixed)	2.42	1.7×10^{21}	3.63	0.02	0.41	2.29×10^3	5.90×10^3
STIS (N_{eff} fixed)	3.42	6.5×10^{21}	7.77	0.02	0.40	2.30×10^3	2.10×10^4

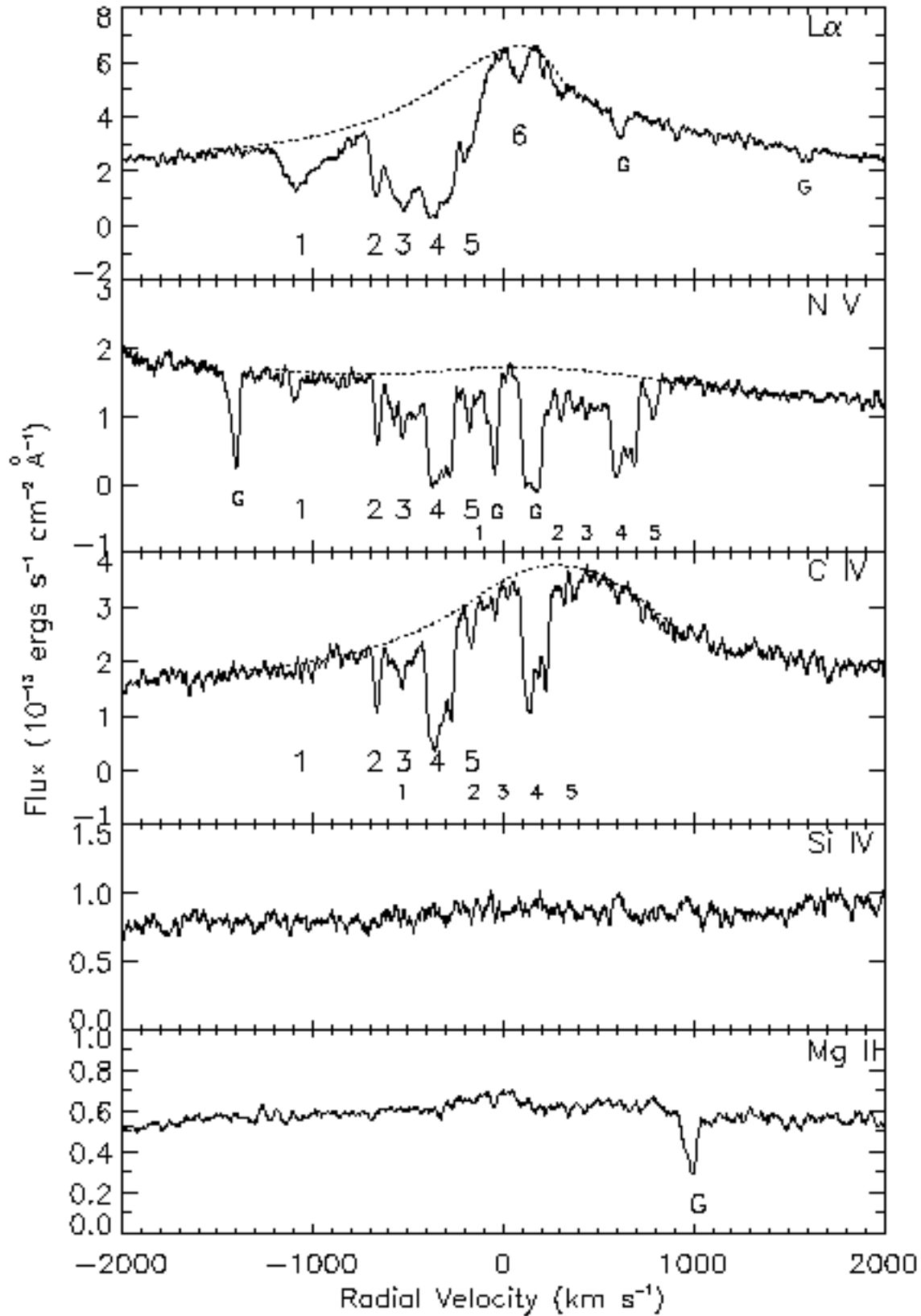


Fig. 1.